



## A Comparative Corrosion Study of Al/Al<sub>2</sub>O<sub>3</sub>-SiC Hybrid Composite Fabricated by Accumulative Roll Bonding (ARB)

Mohsen Reihanian<sup>\*1</sup>, Seyyed Mohammad Lari Baghal<sup>1</sup>, Fateme Keshavarz Haddadian<sup>1</sup>, Mohammad Hosein Paydar<sup>2</sup>

<sup>1</sup>Department of Materials Science and Engineering, Faculty of Engineering, Shahid Chamran University of Ahvaz, Iran

<sup>2</sup>Department of Materials Science and Engineering, School of Engineering, Shiraz University, Shiraz, Iran

Received: 22 February 2016; Accepted: 30 May 2016

Corresponding author email: [m.reihanian@scu.ac.ir](mailto:m.reihanian@scu.ac.ir)

### ABSTRACT

In this study, the Al/Al<sub>2</sub>O<sub>3</sub>-SiC hybrid composite was produced by accumulative roll bonding (ARB). In the first and the second cycles, the particles were uniformly poured between the Al strips during each ARB cycle. In the subsequent cycles, ARB was repeated up to six cycles without adding the particles between the layers. After the total eight cycles, the particles were distributed uniformly without agglomeration in the Al matrix. The corrosion behavior of the hybrid composite was investigated and compared with that of the annealed and ARB processed Al. The corrosion tests were conducted by the potentiodynamic and electrochemical impedance spectroscopy tests in 3.5 wt-% NaCl solution. The anodic potential of the pure Al processed by ARB was more positive than that of the annealed Al while its corrosion current density was higher. The corrosion potential of the hybrid composite was somewhere between the annealed Al and ARB processed Al. The hybrid composite exhibited the lowest current density and the highest charge transfer resistance. The increased corrosion resistance of the hybrid composite was attributed to the inert character of the Al<sub>2</sub>O<sub>3</sub> and SiC particles because these particles could decrease the active sites of the material surface and impeding the corrosive attacks.

**Keywords:** Accumulative roll bonding (ARB); Corrosion; Metal-matrix composites (MMCs); Microstructure.

### 1. Introduction

Metal matrix composites (MMCs) have attracted in the research and industrial applications due to their unique properties [1]. Conventionally, a variety of methods has been successfully employed for production of MMCs [2]. Plastic deformation is generally used to shape mechanical parts and control their mechanical properties. It can also be used to join parts of sufficient ductility without the external heat [3]. The fabrication of composite sheets by cold roll bonding (CRB) has also revealed rapid development in recent years due to its unique

service performance [4]. The effects of conventional rolling and cross-shear rolling (rolls with different peripheral speeds) on the roll force and bonding strength have been previously investigated [5]. The tearing of Al sheet during the peel test indicate that the bond strength of the roll bonded sheets through 38% reduction reaches the strength of Al, which is an advantage of the developed sheets [6].

Recently, fabrication of MMCs by accumulative roll bonding (ARB) has attracted considerable attention because, in addition to composite production, it produces ultrafine-grained materials

with unique physical and mechanical properties [7]. ARB is one type of severe plastic deformation (SPD) method that consists of multiple cycles of stacking, rolling and cutting of the metal strips [8]. In order to produce particulate MMCs by ARB, ceramic particles are added between the metal strips through the initial cycles. After imposing a critical reduction, a uniform distribution of particles is achieved in the matrix [9]. Recently, some efforts have been directed toward fabricating the hybrid composites that contains two different types of the particles [10].

To date, the microstructure and mechanical properties of particulate MMCs fabricated by ARB have been widely characterized by lots of works. However, the corrosion behavior of pure metals [11-13] and MMCs [14, 15] processed by ARB has attracted slight attentions. For example, Wei et al. [11] investigated the corrosion behavior of ARB processed Al-Mn alloy in 3.5% NaCl artificial seawater for 168 h and concluded that the size and the amount of pitting corrosion in ARB processed Al decreased compared with the coarse-grained Al alloy. The pitting corrosion susceptibility of 5052 Al alloy before and after ARB was examined in 3.5 wt% NaCl solution by Naeini [12]. They showed that pitting corrosion resistance diminished with increasing the number of ARB cycles and contributed it to the microstructure refinement and increasing the defect density. Fattah-alhosseini and Imantalab [13] pointed out that ARB could provide a better conditions for forming the passive films in pure copper in 0.01 M borax solution. Darmiani et al. [14] studied the corrosion behavior of Al/SiC nano-composite produced by ARB in 3.5 wt% NaCl solution. They observed that ARB caused the pitting corrosion resistance to increase due to the uniform distribution of SiC in matrix and its refinement. Kadkhodae et al [15] demonstrated that as a result of ARB, the general corrosion resistance of Al/nanosilica nanocomposites decreased, compared to the pure Al. In addition, they found that by increasing ARB cycles and the amount of the silica nanoparticles, the corrosion resistance of the nanocomposites increased.

The microstructure evolution during ARB has been vastly investigated (particularly for Al and its alloys) in the existing literature [16-19]. These early publications provide a direct demonstration of the potential of using ARB in the production of sheet metals with grain sizes in the sub-micrometer range. The results of this work will be helpful in

understanding the corrosion behavior of the Al/Al<sub>2</sub>O<sub>3</sub>-SiC hybrid composite alongside with its promise mechanical properties [10]. The present work is an attempt to study the corrosion behavior of the Al/Al<sub>2</sub>O<sub>3</sub>-SiC hybrid composite fabricated by ARB and its comparison to that of the annealed and ARB processed Al.

## 2. Materials and method

As received commercially pure Al (AA1050) was used in the form of sheet with the thickness of 0.5 mm as the matrix material. The strips were cut into 150 mm × 70 mm and annealed at 400° C for 2 h. A mixture of Al<sub>2</sub>O<sub>3</sub> and SiC particles were used as reinforcements. The average size of Al<sub>2</sub>O<sub>3</sub> and SiC was about 1 μm and 5 μm, respectively. After the surface preparation, ARB process was carried out in two steps [10]. In the first (Fig.1a), 1 vol-% of the particles was uniformly distributed between four Al strips. The stacked strips were fastened at both ends by copper wires and roll bonded through a 50% reduction in thickness at ambient temperature without lubrication. The roll-bonded strip was then cut into two halves while the remaining 1 vol-% of particles was dispersed between them, stacked and roll-bonded again under the same conditions. At this stage, the total volume fraction of particles reaches to 2 vol-%. In the second step (Fig.1b), ARB was repeated up to six cycles without adding the particles between the layers. The rolling machine had the capacity of 20 tons and rolling diameter of 170 mm. The rolling speed was set to 12 rpm.

The corrosion tests were carried out in a 3.5 wt-% NaCl aqueous solution at room temperature. The samples were immersed into the electrolyte for about 30 min to stabilize the open-circuit potential,  $E_o$ . The sweeping rate was 50 mV min<sup>-1</sup> for all potentiodynamic tests. The values of the corrosion potential,  $E_{corr}$ , and the corrosion current density,  $I_{corr}$ , were calculated from the intersection of the cathodic and anodic Tafel curves extrapolated from the anodic and cathodic polarization curves. The electrochemical impedance spectroscopy (EIS) test was used to simulate the map and element of corrosion circuit with the help of Z-view software.

## 3. Results and discussion

Fig.2 illustrates the microstructure of the hybrid composite at low and high magnification. The Al<sub>2</sub>O<sub>3</sub> and SiC particles are indicated by arrows. The critical reduction needed to get a uniform

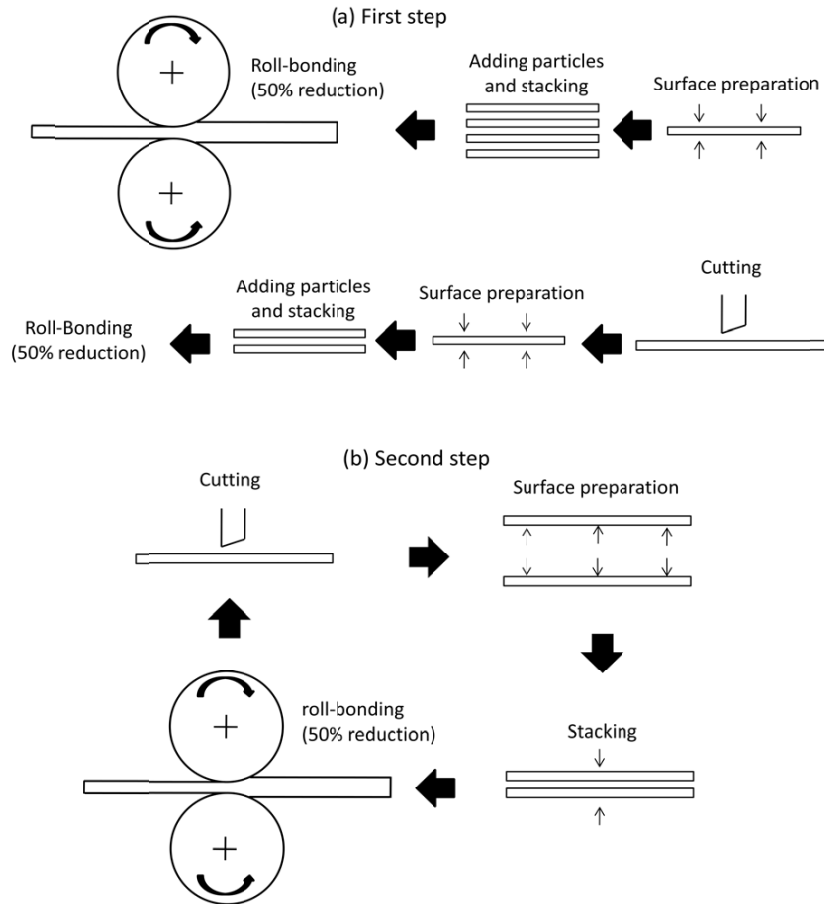


Fig.1- Schematic illustration of ARB process used to fabricate the hybrid composite

distribution of particles in a hybrid composite is determined by [9]

$$R_c = 1 - \left[ \frac{\pi}{6(f_A d_B^3 + f_B d_A^3)} \right]^{1/3} \left( \frac{d_A d_B}{t_0} \right) \quad (1)$$

where  $d$  is the particle size,  $f$  is the volume fraction and  $t_0$  is the initial thickness of the layers. The subscripts A and B stand for particles A and B, respectively. By inserting  $d_A = 1 \mu m$ ,  $d_B = 5 \mu m$ ,  $f_A = f_B = 0.01$  and  $t_0 = 0.5 m$ , the critical reduction needed to get a uniform distribution of particles is predicted as 0.9925. The total reduction that is experimentally imposed after eight ARB cycles is 0.998, which is higher than that of the predicted value for the given conditions. Therefore, a uniform distribution of particles is expected by the model [9] that is confirmed by the SEM images of Fig.2. During ARB, the number of layers increases and their thickness decreases. At the same time, Al matrix is deformed plastically and extruded

between the particles. This leads to separation and movement of the particles from interfaces into the bulk of the Al matrix. In addition, elongation of the particle clusters in the rolling direction can increase the distance between the particles inside the clusters, changing the dense clusters into the diffuse clusters [20].

The potentiodynamic polarization curves recorded for the annealed Al, ARBed Al and the hybrid composite fabricated by the ARB are shown in Fig.3. The calculated parameters extracted from the polarization diagrams are given in Table 1. All samples show an active behavior in the anodic potential, indicating the formation of a non-protective passive film. In general, the surface of the Al and its alloys is covered by a passive film of alumina due to the chemical reaction between the Al and the air. Nevertheless, Al and its alloys are sensitive to pitting corrosion in aqueous media, which is hazardous for formation of the protective passive film. The anodic potential of the ARBed

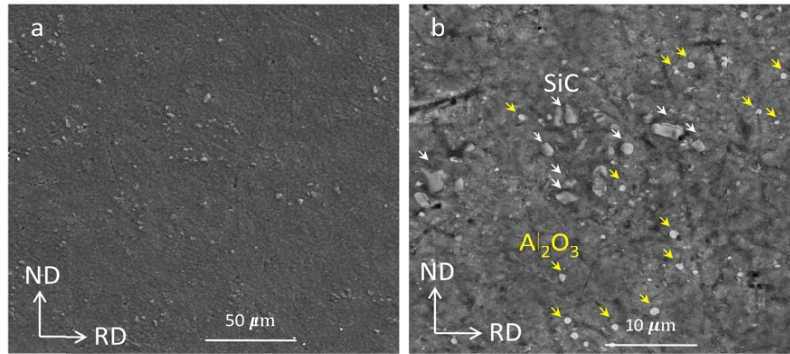


Fig.2- SEM micrograph of the hybrid composite at (a) low and (b) high magnification

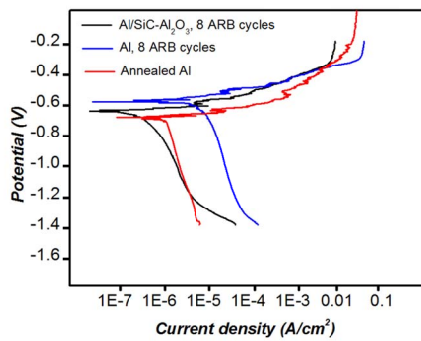


Fig.3- Potentiodynamic polarization curves of the annealed Al, ARBed Al and hybrid composite

Al is more positive than that of the annealed Al while its corrosion current density is higher. The corrosion potential of the hybrid composite is somewhere between the annealed Al and ARB processed Al and it shows the lowest corrosion current density (Table 1). Generally, the corrosion potential,  $E_{corr}$ , represents a thermodynamic characteristic of a given metal–electrolyte system rather than the kinetics of material corrosion whereas the corrosion current density,  $I_{corr}$ , reflects the corrosion rate more accurately. These results indicate that the corrosion resistance of the hybrid composite fabricated by ARB can be improved in comparison to the pure Al processed by ARB.

Fig.4 represents Nyquist plots and the equivalent electrical circuit applied for simulation of EIS tests, respectively. The impedance spectra of all

specimens consist of two capacitive loops at higher frequencies and a semicircle at lower frequencies. The first capacitive loop is corresponding to the charge transfer of the corrosion process and to the formation of oxide layer. The second capacitive loop is assigned to the interfacial reactions, particularly, the reaction of Al oxidation at the metal/oxide/electrolyte interface. The presence of the semicircle at lower frequencies is due to the diffusion of the chemical species from the oxide layer on the surface.

This behavior is clearly evidenced by observing a  $45^\circ$  straight tail at the end of Nyquist diagram of the annealed Al, which is the characteristic of Warburg impedance. The equivalent circuit model in Fig.4 is proposed to simulate the corrosion behavior of the Al samples having a defective oxide layer.

The calculated equivalent circuit parameters are listed in Table 2; where  $R_{sol}$ ,  $C_{coat}$ ,  $R_{coat}$ ,  $C_{dl}$ ,  $R_{ct}$  and  $W$  represent the electrolyte solution resistance, capacitance of the oxide layer, resistance of the oxide layer, capacitance of the double layer, charge transfer resistance of the double layer and Warburg impedance, respectively. The charge transfer resistance is the resistance of the metal atom that is ionized when it is in contact with the electrolyte. The higher value of  $R_{ct}$  represents the higher corrosion resistance.

According to Table1 and Table 2, the pure Al processed by ARB exhibits the highest value of  $I_{corr}$  and the lowest value of  $R_{ct}$ , indicating that ARBed

 Table 1- The calculated values of  $E_{corr}$ ,  $I_{corr}$ ,  $\beta_a$  and  $\beta_c$  for the polarization diagrams

Material	$E_{corr}$ (V)	$I_{corr}$ ( $\mu A/cm^2$ )	$\beta_a$	$\beta_c$
Annealed Al	-6.9	4.54	45	180
ARBEd Al	-5.6	9.34	63	125
Al/Al <sub>2</sub> O <sub>3</sub> -SiC hybrid composite	-6.4	0.35	67	112

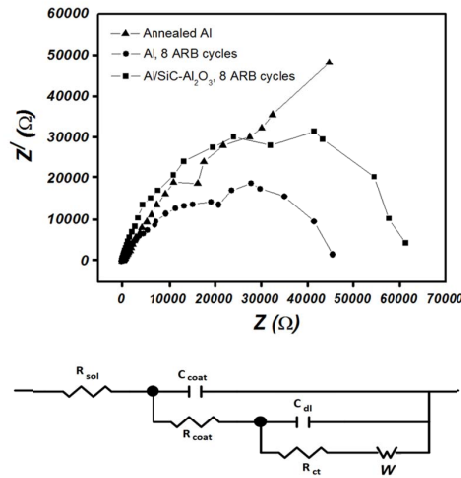


Fig.4- Nyquist plots and the equivalent electrical circuit applied for simulation of EIS tests

Table 2- The calculated values of  $R_{sol}$ ,  $C_{coat}$ ,  $R_{coat}$ ,  $C_{dl}$ ,  $R_{ct}$  and  $W$  for the impedance diagrams

Material	$R_{sol}$ ( $\Omega$ )	$C_{coat}$ ( $\mu F / cm^2$ )	$R_{coat}$ ( $k\Omega$ )	$C_{dl}$ ( $\mu F / cm^2$ )	$R_{ct}$ ( $k\Omega$ )	$W$ ( $\Omega / cm^2$ )
Annealed Al	8.5	8.3	7.5	8	40	1500
ARBed Al	12	6.1	9.3	9.6	23	340
Al/Al <sub>2</sub> O <sub>3</sub> -SiC hybrid composite	10.5	3.4	14.4	5	45	280

Al has the lowest corrosion resistance. These results demonstrate that there is a good agreement between the potentiodynamic polarization tests and the electrochemical impedance spectroscopy. The lowest corrosion resistance of the ARBed Al may be due to the formation of fine grains and the increase in strain energy after ARB. These microstructural features cause the rate of cathodic reaction of the pure Al to be enhanced.

The increased density of the active sites such as grain boundaries and triple junctions raises the

chemical activity of the surface. This is consistent with the higher cathodic polarization current density of ARBed Al, which is an indicative of the higher reduction rate of  $H^+$  ions to  $H_2$  atoms due to the cathodic reaction. On the other hand, in contrast to the results of Fig.4, it is expected that the increased energy state and the active sites in the ARB processed Al must shift the corrosion potential to more negative values. This argument can be explained by the fact that although the presence of the active sites is effective on the corrosion potential, however, both the oxidation and reduction reactions should be considered in the equilibrium condition during the corrosion. Generally, corrosion occurs at a potential, denoted by  $E_{corr}$ , where the oxidation rate,  $I_{corr}$ , is equal to the reduction rate. As shown in Fig.5, this potential can be graphically determined by the intersection of the partial oxidation polarization and the partial reduction polarization curves on the potential versus the current density plot [21]. For a given partial oxidation curve, the increase in the rate of the reduction reaction can transfer the intersection point to the upper right of the diagram, leading to the simultaneous increase in  $E_{corr}$  and  $I_{corr}$  values (such as pure Al processed by ARB). In addition,

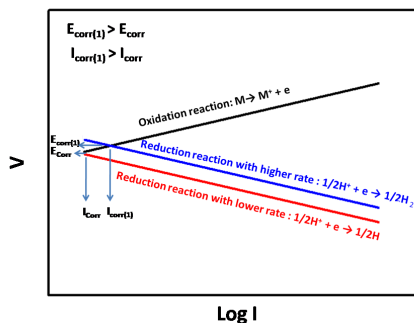


Fig. 5- Schematic illustration of potential versus current density plot for partial oxidation and reduction reaction engaged in corrosive process

the higher ability to form the oxide film can also lead to the higher anodic potential of the ARB processed Al because passivation starts primarily at the lattice defects that are higher in this sample.

The anodic potential of the hybrid composite is nobler than that of the annealed Al but it has the lowest cathodic current density, indicating that the hybrid composite has the ability to form an oxide layer similar to ARBed Al but with the lowest cathodic reaction rate. These results are confirmed by the data presented in Table 1 and Table 2 where the hybrid composite shows the lowest value of the  $I_{corr}$  and the highest  $R_{cp}$  respectively. The conclusion is drawn that the presence of the  $Al_2O_3$  and SiC ceramic particles can improve the corrosion resistance of the Al after ARB. The inert effect of the particles causes the activity of the surface and the cathodic reaction rate to decrease. A decrease in the cathodic reaction rate can shift the equilibrium condition of the corrosion process to the lower value of  $I_{corr}$ . In addition, the lower value of  $E_{corr}$  can be attributed to the shift of the intersection point of the partial oxidation and reduction curves to the lower left of the potential versus the current density plot due to the decrease in the rate of cathodic reaction.

#### 4. Conclusions

The corrosion behavior of the Al/ $Al_2O_3$ -SiC hybrid composite produced by ARB was investigated and compared to that of the annealed and ARBed Al. The following results can be obtained:

1. A hybrid composite with a uniform distribution of particles is achieved after eight ARB cycles. The particles are distributed without agglomeration because, after eight ARB cycles, the imposed reduction is larger than the critical reduction predicted by the model.

2. The ARB decreases the corrosion resistance of the Al due to the formation of fine grains and the increase in the strain energy of the material. These microstructural features cause the rate of cathodic reaction to increase after ARB.

3. The hybrid composite exhibits the lowest corrosion current density and the highest charge transfer resistance. The highest corrosion resistance of the hybrid composite is due to the inert effect of the particles that causes the chemical activity of the surface and the cathodic reaction rate of the hybrid composite to decrease.

#### Acknowledgements

The authors would like to acknowledge the financial support of Shahid Chamran University of Ahvaz through the Grant Number EN-92-874095.

#### References

1. Miracle DB. Metal matrix composites – From science to technological significance. *Composites Science and Technology*. 2005;65:2526-40.
2. Ralph B, Yuen HC, Lee WB. The processing of metal matrix composites — an overview. *Journal of Materials Processing Technology*. 1997;63:339-53.
3. Mori K-i, Bay N, Fratini L, Micari F, Tekkaya AE. Joining by plastic deformation. *CIRP Annals - Manufacturing Technology*. 2013;62:673-94.
4. Li L, Nagai K, Yin F. Progress in cold roll bonding of metals. *Science and Technology of Advanced Materials*. 2008;9:023001.
5. Pan D, Gao K, Yu J. Cold roll bonding of bimetallic sheets and strips. *Materials Science and Technology*. 1989;5:934-9.
6. Akramifard HR, Mirzadeh H, Parsa MH. Cladding of aluminum on AISI 304L stainless steel by cold roll bonding: Mechanism, microstructure, and mechanical properties. *Materials Science and Engineering: A*. 2014;613:232-9.
7. Alizadeh M, Paydar MH. Fabrication of nanostructure Al/SiC composite by accumulative roll-bonding (ARB) process. *Journal of Alloys and Compounds*. 2010;492:231-5.
8. Saito Y, Utsunomiya H, Tsuji N, Sakai T. Novel ultra-high straining process for bulk materials—development of the accumulative roll-bonding (ARB) process. *Acta Materialia*. 1999;47:579-83.
9. Reihanian M, Bagherpour E, Paydar MH. On the achievement of uniform particle distribution in metal matrix composites fabricated by accumulative roll bonding. *Materials Letters*. 2013;91:59-62.
10. Reihanian M, Keshavarz Hadadian F, Paydar MH. Fabrication of Al-2vol% $Al_2O_3$ /SiC hybrid composite via accumulative roll bonding (ARB): An investigation of the microstructure and mechanical properties. *Materials Science and Engineering: A*. 2014;607:188-96.
11. Wei W, Wei KX, Du QB. Corrosion and tensile behaviors of ultra-fine grained Al-Mn alloy produced by accumulative roll bonding. *Materials Science and Engineering: A*. 2007;454-455:536-41.
12. Naeini MF, Shariat MH, Eizadjou M. On the chloride-induced pitting of ultra fine grains 5052 aluminum alloy produced by accumulative roll bonding process. *Journal of Alloys and Compounds*. 2011;509:4696-700.
13. Fattah-alhosseini A, Imantalab O. Effect of accumulative roll bonding process on the electrochemical behavior of pure copper. *Journal of Alloys and Compounds*. 2015;632:48-52.
14. Darmiani E, Danaee I, Golozar MA, Toroghinejad MR. Corrosion investigation of Al-SiC nano-composite fabricated by accumulative roll bonding (ARB) process. *Journal of Alloys and Compounds*. 2013;552:31-9.
15. Kadhodaee M, Babaiee M, Danesh Manesh H, Pakshir M, Hashemi B. Evaluation of corrosion properties of Al/nanosilica nanocomposite sheets produced by accumulative roll bonding (ARB) process. *Journal of Alloys and*

- Compounds. 2013;576:66-71.
16. Li BL, Tsuji N, Kamikawa N. Microstructure homogeneity in various metallic materials heavily deformed by accumulative roll-bonding. *Materials Science and Engineering: A*. 2006;423:331-42.
  17. Kamikawa N, Tsuji N, Huang X, Hansen N. Quantification of annealed microstructures in ARB processed aluminum. *Acta Materialia*. 2006;54:3055-66.
  18. Huang X, Tsuji N, Hansen N, Minamino Y. Microstructural evolution during accumulative roll-bonding of commercial purity aluminum. *Materials Science and Engineering: A*. 2003;340:265-71.
  19. Lee SH, Saito Y, Sakai T, Utsunomiya H. Microstructures and mechanical properties of 6061 aluminum alloy processed by accumulative roll-bonding. *Materials Science and Engineering: A*. 2002;325:228-35.
  20. Yazdani A, Salahinejad E, Moradgholi J, Hosseini M. A new consideration on reinforcement distribution in the different planes of nanostructured metal matrix composite sheets prepared by accumulative roll bonding (ARB). *Journal of Alloys and Compounds*. 2011;509:9562-4.
  21. Fontana MG. *Corrosion Engineering*: Tata McGraw-Hill; 2005.